Chapter 9

Solar-Powered Electrochemical Production of Molecular Hydrogen from Water

Sections reprinted with permission from Park, H.; Vecitis, C. D.; Choi, W.; Weres, O.; Hoffmann, M. R. *Journal of Physical Chemistry C* **2008**, *112*, 4, 885–889.

Abstract

Electrochemical water splitting powered by conventional electricity or photovoltaic arrays produces molecular hydrogen at the cathode while organic compound oxidation under mild conditions takes place at the anode in competition with the production of oxygen. An electrolytic cell, which is based on the coupling of bismuth-doped titanium dioxide anodes (BiO_x-TiO_2) with stainless steel cathodes (SS), is characterized in terms of hydrogen production efficiency and organic compound degradation. In the solar-powered PV-electrochemical system, the production of molecular oxygen at the anode is suppressed by the simultaneous oxidation and mineralization of organic compounds dissolved in water. In addition, the anodic oxidation of organic substrates has a synergistic effect on hydrogen production at the cathode that results in a 53% increase in the energy efficiency for H_2 generation at circum-neutral pH in the presence of dilute electrolyte solutions.

Introduction

At the present time, the majority of industrial-scale hydrogen is produced by steam-methane reformation (SMR), even though the high temperature conversion of methane to hydrogen results in the concomitant production of carbon monoxide and carbon dioxide at a weight ratio of CO_2 to H_2 equal to 2.5. As a consequence, SMR has a relatively large carbon footprint. Carbon-free water electrolysis is considered to be less attractive given the rising costs of electricity[1-3]. However, the direct utilization of solar light for hydrogen production through photocatalytic[4] or photo-electrochemical[5,6] water splitting may provide an economically viable alternative source of hydrogen in the future.

There have been several previous reports of electrolysis systems powered nominally by photovoltaic arrays[7-9]. The PV arrays are used to convert solar light to electricity in order to power alkaline (e.g., 27% KOH at pH 14.7) electrolyzers for producing hydrogen gas. However, these systems are thought to be impractical in that the cost of hydrogen is greater than conventional DC-electrolysis, which in turn, is more expensive than SMR.

Narayanan et al. describe a DC-powered hybrid system that drives a methanol fuel cell in reverse[10], while Soler et al. report on a solar-powered photo-Fenton process that produces hydrogen noncatalytically under severe condition with a limited number of organic substrates[11]. Mathieson et al. described a hybrid electrolytic system that functions via the induced corrosion of the anode to release the corresponding metal ions to solution, which lead to the coagulation and subsequent removal of high-molecular-weight organic compounds from water[12]. Drew et al. reported TiO_2/Ru-Pt hybrid catalyst for boosting fuel cell performance[13].

In this letter, we report on a hybrid photovoltaic electrochemical reactor that results in the simultaneous production of molecular hydrogen via water splitting at stainless steel cathodes, while organic substrates are oxidized at metal-doped TiO_2 anodes (Scheme 9.1). Semiconductor electrodes have been used to drive the electrochemical splitting of water into hydrogen and oxygen. However, we have previously demonstrated that the oxidation of water via an overall four-electron oxidation can be suppressed by using anodes made with niobium-doped polycrystalline TiO_2 particles attached to metallic titanium plates[14]. Metal-doped TiO_2 electrodes preferentially oxidize water to hydroxyl radical due to the formation of surface titanol (>TiOH) groups on hydrated titanium dioxide surfaces at current efficiencies approaching 50%. In addition, the surface-bound hydroxyl radicals on the semiconductor anodes can be utilized to preferentially oxidize a wide variety of organic and inorganic substrates[14]. In this letter, we characterize the electrochemistry of a mixed-metal oxide anode that is based on a mixture of bismuth oxide and Bi-doped TiO_2 that is coupled to a stainless-steel cathode and powered by a photovoltaic panel.

The BiO_x-TiO_2-coated titanium anode[15] and stainless steel cathode were immersed in an electrolyte solution (e.g., 50 mM NaCl) in a reactor with a total volume of either 200 mL in a single electrode couple or 20 L with multiple electrode couples. Organic substrates were mixed into the background electrolyte solutions or added during the course of electrolysis. A constant cell voltage or current was applied to the electrodes either with a DC power supply (HP 6263B and 6260B) or with a commercial amorphous silicon PV panel (Silicon Solar, Inc.) that has a power rating of 6.4 W with a peak output potential, E_{peak} = 8–10V, and a peak current of I_{peak} = 0.95A for an active surface area of 1280 cm^2 (Scheme 9.1). The theoretical maximum solar-to-electric energy efficiency is

estimated to be 4.5% according to the specifications of the PV manufacturer. Solar radiation was monitored by a pyranometer (Apogee) connected to a data-logger (Campbell Scientific). Cell voltage (E_{cell}) and current (I_{cell}) were monitored with a digital multimeter (Fluke). The current efficiencies and the energy efficiencies are obtained as follows in eqs. 9.1 and 9.2.

$$\text{Current efficiency (\%)} = \frac{\text{\# molecules produced } (H_2,\ O_2,\ \text{or } CO_2) \text{ or degraded (phenol)}}{\text{\# electrons}} \times n \times 100 \quad (9.1)$$

$$H_2 \text{ production energy efficiency (\%)} = \frac{(39 W \cdot h/g \times H_2 \text{ rate} \times 2 g/mol)}{E_{cell} \times I_{cell}} \times 100 \quad (9.2)$$

where n = 2 and 4 for hydrogen and oxygen production cathodic current (CE) efficiencies, respectively. For anodic current efficiencies, n = 1 for one-electron oxidation of phenol, and n = 14/3 for complete mineralization from phenol carbon to carbon dioxide.

The electrolytic reactors were sealed to the atmosphere and the headspace gas was extracted at a known rate by a peristaltic pump. The extracted headspace gas was pulled through a stainless steel membrane into the vacuum chamber (5.0×10^{-6} torr), evacuated by a membrane pump and a turbo pump (Pfeiffer Vacuum), where it was ionized by high-energy electrons and analyzed by quadrupole mass spectrometry (Balzers). The volume percent of the headspace was calculated by assuming that the observed signal intensity was directly proportional to the ion current measured by the mass spectrometer (i.e., the transfer of all gases through the membrane and their 70 eV electron ionization cross-sections were roughly equivalent). This assumption is validated by the fact that ambient air was measured to be 77% nitrogen, 17% oxygen, 5% water vapor, and 1% argon.

Aqueous organic compounds including intermediates were analyzed by high performance liquid chromatography (HPLC, Agilent 1100 series) with separation on a

C18 column. The eluent composition was 55% Milli-Q water (0.1 wt% acetic acid) and 45% acetonitrile at flow rate of 0.7 mL min^{-1}. Analyte concentrations were monitored by UV-Vis spectrophotometry. Total organic carbon measurements were made with an OI Analytical Aurora Model 1030 TOC analyzer coupled to an autosampler (OI Analytical Model 1096).

The composite BiO_x-TiO_2 anodes, when coupled with stainless steel (SS) cathodes have an inherent potential ranging from + 0.2 to + 0.5 V, due to the formation of a space-charge layer within the TiO_2 particles bound to the titanium substrate. Water splitting and current flow commence at an applied cell voltage of + 2.0 V, with an observed a linear correlation between the measured rates of H_2 and O_2 production, eq. 9.3 (Figure 9.1).

$$2\,H_2O \xrightarrow{E > +2.1\,V} 2\,H_2 + O_2 \qquad (9.3)$$

The H_2/O_2 mole ratio for the electrolysis of pure water (i.e., without added substrates) depends on the background electrolyte. In the case of sodium sulfate (50 mM), the observed H_2/O_2 mole production ratio is 5.2, while in the presence of sodium chloride (50 mM) the corresponding mole ratio (H_2/O_2) is increased to 7.6 (Figure 9.1). The sharp departures from a theoretical 2 to 1 mole ratio for water splitting indicate that electrochemical reaction products or intermediates other than oxygen are being formed at the semiconductor anode. These reactions include the oxidation of surface-bound hydroxyl groups of hydrated TiO_2 to produce hydroxyl radicals (i.e., eq. 9.4, as depicted in Scheme 9.1), as well as the oxidation of the background electrolyte (e.g., Cl^-; eq. 9.5).

$$\mathbf{> Ti - OH \rightarrow > Ti - OH^{\bullet} + e^-} \qquad (9.5)$$

At applied potentials greater than 2.0 V, the one-electron oxidation of chloride ($E°(Cl^{\bullet}/Cl^{-})$ = 2.55 V vs. NHE) and sulfate ($E°(SO_4^{\bullet-}/SO_4^{2-})$ = 2.43 V vs. NHE) are competitive with water oxidation.

When powered by a photovoltaic (PV) panel, the cell voltage (E_{cell}) of the reactor increases to +4 V with a corresponding current (I_{cell}) close to 0.9 A (i.e., 30 mA cm^{-2}), as shown in Figure 9.2. The voltage and current of the electrodes are nearly constant under steady sunlight irradiation at a measured solar flux of 1100 $W \cdot m^{-2}$. The hybrid PV-electrochemical reactor system produces hydrogen at a rate of 0.18 mmol min^{-1} and oxygen at rate of 0.028 mmol min^{-1}, which corresponds to a ratio of the rates of production (i.e., a H_2/O_2 mole ratio) that is near 7.

With the addition of phenol, the hydrogen production rate is enhanced by 20 to 30% and the oxygen production rate is slightly decreased. The overall energy efficiency for H_2 production ranges from 30 to 40% depending on the PV panel output energy. The DC-powered current efficiency for the hybrid electrolysis ranges from 70 to 95%, while the corresponding energy efficiencies for H_2 production range from 36 to 61%, depending on operating conditions (Table 9.1). These values compare favorably with industrial-scale electrolysis employing alkaline or proton exchange membrane electrolyzers with reported energy efficiencies ranging from 56 to 73%. Our hybrid PV- and DC-powered systems operate at comparable efficiencies; however, they have distinct advantages over commercial electrolytic devices, in that the hybrid system is efficient at low electrolyte concentrations at circum-neutral pH under ambient temperature and pressure. The overall solar-to-hydrogen energy efficiency is thereby limited by the actual solar light energy-to-

electric power conversion efficiency (ε) of the specific PV system that is used to drive electrolytic water splitting with semiconductor electrodes.

In the case of phenol, oxidative degradation (> 99%) is achieved within 10 min ($t_{1/2}$ ~ 1 min) (Figure 9.2). The electrolytic oxidation follows first-order kinetics with the eventual conversion of the phenolic carbon into CO_2. This overall process can be repeated with each successive addition of phenol to the hybrid PV-electrolytic reactor. The phase-delay for the detectable production of carbon dioxide relative to the disappearance of phenol indicates that carbon-containing intermediates are produced and are involved in further competitive reactions at the semiconductor anode. Reaction intermediates found during electrolysis at a constant current density of 14 mA cm^{-2} with NaCl as the background electrolyte included mono-, di-, and tri-chlorophenol (Figure 9.3). When added individually, the chlorinated phenols are destroyed in the following order of relative electrochemical reactivity: 2,4,6-trichlorophenol (3.74) > 2,6-dichlorophenol (1.84) > 2,4-dichlorophenol (1.38) > phenol (1.0) > 2-chlorophenol (0.78) > 4-chlorophenol (0.57) (Table 9.1), where the numbers in parenthesis represent reaction rates relative to phenol. The trichlorophenol reaction intermediate undergoes a sequential dechlorination through a cyclopentene intermediate, followed by production of simple aliphatic acids that are formed after ring opening. The aliphatic acid intermediates are then oxidized to CO_2 by surface-bound hydroxyl radicals that are produced at the anode (R1 in Scheme 9.1). Due to the competitive reactions of phenol and intermediates at the anode, the one-electron oxidation current efficiency for the oxidation of phenol is 10%, even though the cathodic current efficiency for hydrogen production is close to 70%. Production of the intermediate chlorinated phenols is consistent with the formation of

chlorine radicals such as $Cl^{\bullet}$ and $Cl_2^{\bullet-}$ at the semiconductor anode (R3) when NaCl is used as the background electrolyte. Furthermore, the overall degradation of the chlorinated phenol intermediates leads to the generation of carbon dioxide. For phenol, the total amount of carbon, from carbon dioxide in the PV-connected (30 min, Figure 9.2) and the DC-powered (100 min, Figure 9.3) systems corresponds to around 25% of the phenolic carbon with the time-scale for CO_2 release depending on the initial substrate concentration and reaction conditions (e.g., NaCl concentration). The remainder of the phenolic carbon is present in solution as HCO_2^-, $C_2O_4^{2-}$, HCO_3^-, and CO_3^{2-}.

When phenol is added to the electrochemical reactor, the cell-voltage increases from 4.0 V to 4.2 V, while, at the same time, the cell current appears to be invariant when powered by the PV panel (Figure 9.2). It is clear from the data presented in Figure 9.2 that the addition of phenol increases the hydrogen rate under constant solar radiation (~ 1100 W m^{-2}). Hydrogen production rates are also enhanced with the addition of maleic acid, oxalic acid, catechol, salicylic acid, and a variety of chlorinated phenols as shown in Table 9.1. As depicted in Scheme 9.1, R5 is thermodynamically favored over R4 ($E(Cl_2^{\bullet-}/2Cl^-)$ = +2.3 V; $E(H_2O/H_2,OH^-$ = –0.41 V at pH 7), and competes with R4 for electron at the cathode. However, the added organic compounds react with the intermediate radical species such as $HO^{\bullet}$, $Cl^{\bullet}$, $Cl_2^{\bullet-}$ (R6), which are produced at the anode (R1 & R3) and reduced at the cathode. Since phenol and the other organic substrates react with $HO^{\bullet}$, $Cl^{\bullet}$, and $Cl_2^{\bullet-}$ in solution, as opposed to the cathode surface, more electrons are available for water or proton reduction at the cathode (R4), thereby resulting in increasing H_2 production energy efficiencies of 30 to 53% at lower I_{cell}. In contrast, aliphatic acids increase the observed H_2 production energy efficiencies by a

smaller amount (~ 10%) due to their slower oxidation kinetics and lesser radical (e.g., $Cl_2^{\bullet-}$) reaction rates.

We envision that hybrid PV electrochemical systems could be used for solar-powered water purification, coupled with the generation of a potentially useful and energy rich byproduct. Also, solar light could be directly irradiated to the anode connected to PV to boost the organic oxidation and give much greater synergy effects on the hydrogen production.

Tables

Table 9.1. Electrochemical organic oxidation and hydrogen production[a]

Substrate	k_{obs}[b] (min^{-1})	E_{cell}[c] (V)	H_2[d] (10^{-6} mol/min)		I_{cell} (A)[e]		Energy Efficiency (%)[f]		
			before	after	before	after	before	after	Δ[g]
Maleic acid	-	3.07	70	75	0.29	0.29	45.7	49.4	8.0
Oxalate	-	3.05	71	78	0.30	0.30	45.0	49.6	10.2
Phenol	0.21	3.10	66	86	0.38	0.32	33.0	50.5	53.1
Catechol	0.13	3.25	104	126	0.44	0.42	42.5	54.2	27.3
Hydroquinone	0.96	-	-	-	-	-	-	-	-
Salicylic acid	0.087	3.17	51	63	0.34	0.32	27.8	36.4	31.2
2-ClPhOH	0.17	3.14	67	81	0.34	0.30	36.8	50.2	36.3
4-ClPhOH	0.12	3.18	80	100	0.32	0.30	46.0	61.3	33.3
2,4-ClPhOH	0.29	-	-	-	-	-	-	-	-
2,6-ClPhOH	0.39	-	-	-	-	-	-	-	-
2,4,6-ClPhOH	0.79	-	-	-	-	-	-	-	-

a. 50 mM NaCl used as an electrolyte
b. Observed degradation rates of aqueous pollutants at constant current density of 14 mA cm^{-2}
c. Constant cell voltage
d. Hydrogen production rate before and after addition of substrate (1 mM) at a given voltage
e. Cell current before and after addition of substrate (1 mM) at a given voltage
f. Energy efficiency (EE) for hydrogen production = $(39W{\cdot}h/g\text{-}H_2 \times H_2 \text{ rate} \times 2g/mol\text{-}H_2)/(E_{Cell} \times I_{Cell}) \times 100\%$
g. Δ = (EE after – EE before)/EE before × 100%

Figures

Figure 9.1. Electrochemical H_2 and O_2 production. A) Real-time profiles of H_2 and O_2 as a function of cell voltage (E_{cell}). B) Effects of E_{cell} on cell current (I_{cell}). C) I_{cell} vs. the H_2 and O_2 production rates in different supporting electrolyte medium (Na_2SO_4 vs. NaCl). 50 mM NaCl or 50 mM

A

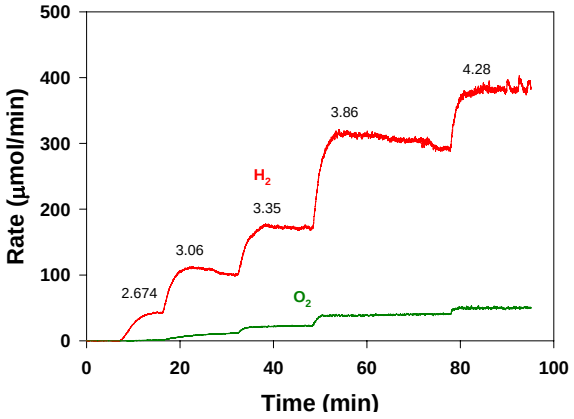

B

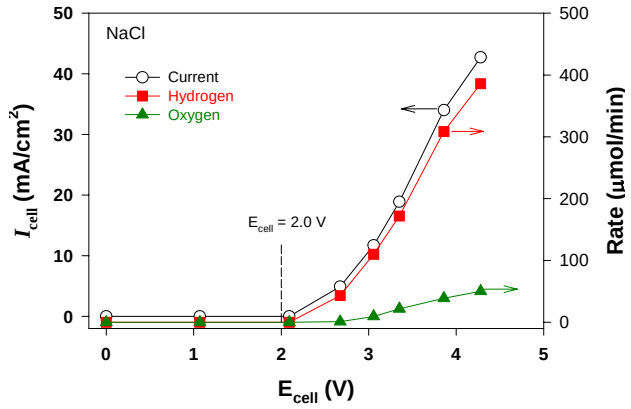

C

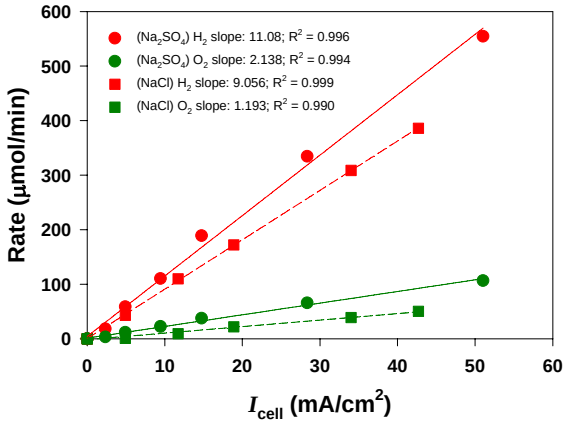

Figure 9.2. Outdoor field test of PV-electrochemical system (April 18th, 2007) on the roof of W.M. Keck Laboratories at the California Institute of Technology. Upper panel: Measurements of temperature and solar radiation (I_S). Middle panel: Measurements of E_{cell} and I_{cell}. Bottom panel: Measurements of phenol degradation (C_t/C_0), CO_2 generation, and hydrogen production. 1 mM of phenol was injected 6 times separately during the electrolysis with 50 mM NaCl

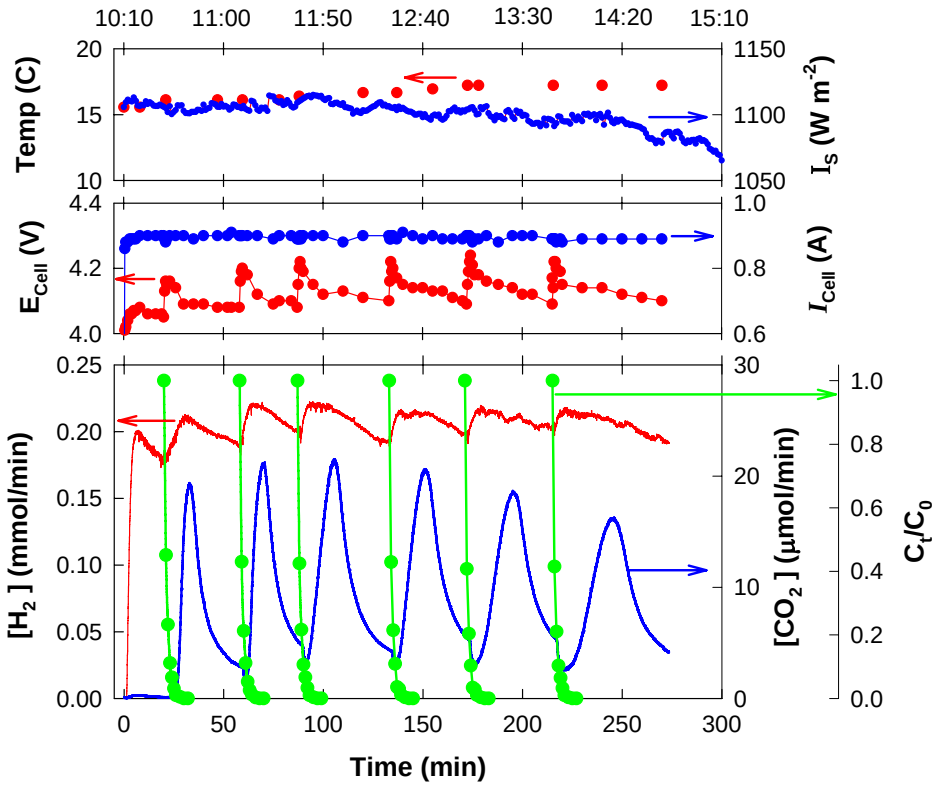

Figure 9.3. Products of electrolytic degradation of 1 mM phenol. TOC change and carbon balance at constant current (14 mA cm^{-2}). Phenol (●), 2-chlorophenol (●), 4-chlorophenol (●), 2,4-dichlorophenol (●), 2,6-dichlorophenol (●), 2,4,6-trichlorophenol (●), CO_2 (—), TOC (■), and carbon balance (□)

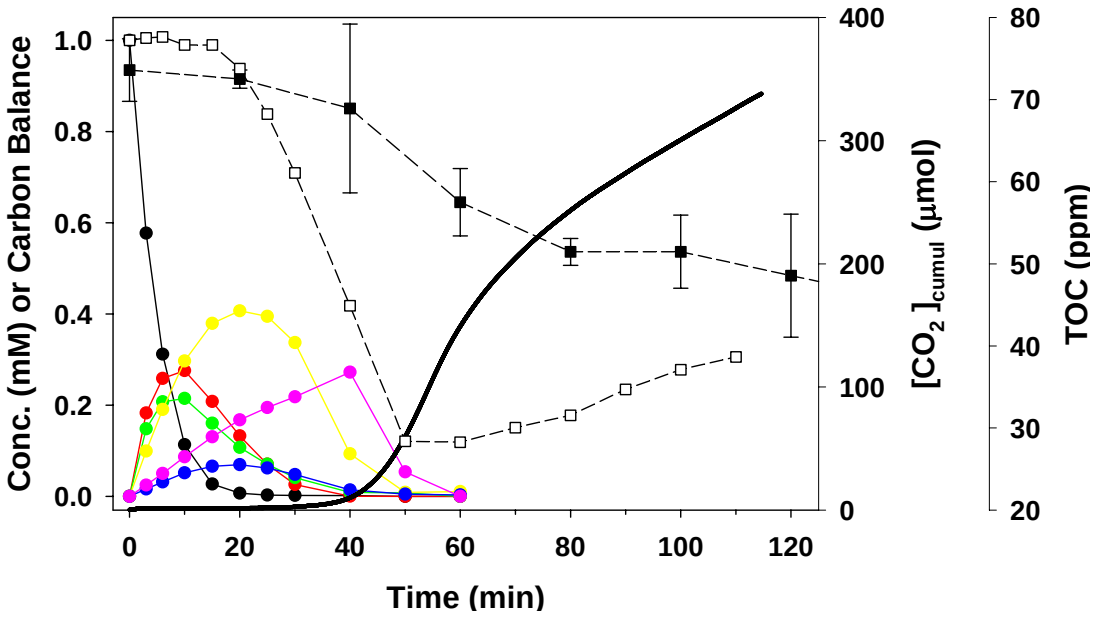

Scheme 9.1. Schematic diagram of the electrochemical setup

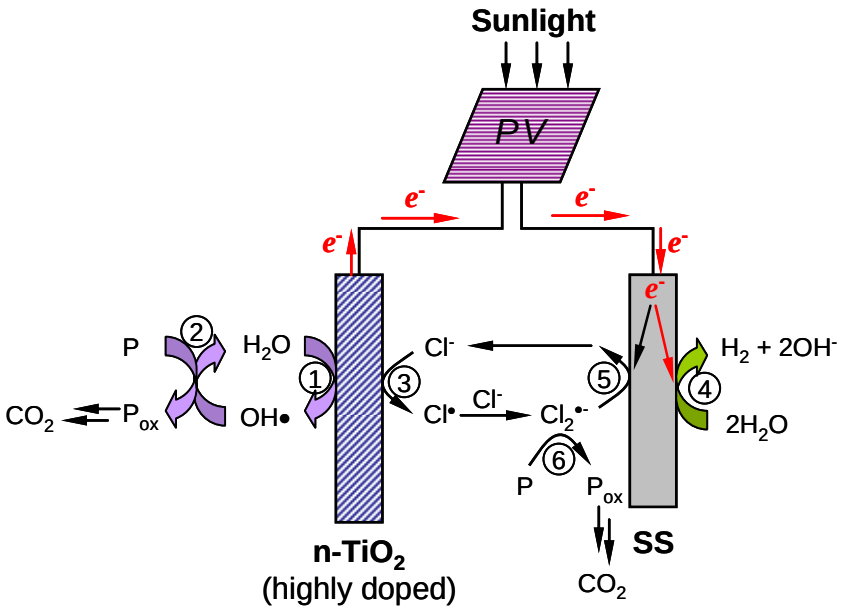

References

1. Turner, J. A. *Science* **2004**, *305*, 972.
2. *Solar and Wind Technologies for Hydrogen Production*, available at http://www.hydrogen.energy.gov/congress_reports.html.
3. Ivy, J. *Summary of Electrolytic Hydrogen Production: Milestone Completion Report*, available at www.nrel.gov/hydrogen/pdfs/36734.pdf.
4. Maeda, K.; Teramura, K.; Lu, D. L.; Takata, T.; Saito, N.; Inoue, Y.; Domen, K. *Nature* **2006**, *440*, 295.
5. Grätzel, M. *Nature* **2001**, *414*, 338.
6. Khaselev, O.; Turner, J. A. *Science* **1998**, *280*, 425.
7. Friberg, R. *Int. J. Hydrogen Energy* **1993**, *18*, 853.
8. Ahmad, G. E.; El Shenawy, E. T. *Renewable Energy* **2006**, *31*, 1043.
9. Lehman, P. A.; Chamberlin, C. E.; Pauletto, G.; Rocheleau, M. A. *Int. J. Hydrogen Energy* **1997**, *22*, 465.
10. Narayanan, S. R.; W., C.; Jeffries-Nakamura, B.; Valdez, T. I. *Hydrogen Generation by Electrolysis of Aqueous Organic Solutions*; U.S. Patent 6,368,492; Apr. 9, **2002**.
11. Soler, L.; Macanas, J.; Munoz, M.; Casado, J. *Int. J. Hydrogen Energy* **2006**, *31*, 129.
12. Mathieson, G.; Langdon, A.; Jamieson, G. *Dev. Chem. Eng. Mineral Process* **2006**, *14*, 71.
13. Drew, K.; Girishkumar, G.; Vinodgopal, K.; Kamat, P.V. *J. Phys. Chem. B* **2005**, *109*, 11851.

14. Kesselman, J. M.; Weres, O.; Lewis, N. S.; Hoffmann, M. R. *J. Phys. Chem. B* **1997**, *101*, 2637.

15. Weres, O. *Electrode with Surface Comprising Oxides of Titanium and Bismuth and Water Purification Process Using This Electrode;* U.S. Patent 0,000,774 A1; Jan. 4, **2007**.